



# Comparative Study of Electrically Assisted Pressure Joining of Aluminum 6061-T6 Alloys and Copper C11000 Alloys

Tu-Anh Bui-Thi<sup>1</sup> · Thanh Thuong Do<sup>1</sup> · Shengwei Zhang<sup>2</sup> · Yijae Kim<sup>3</sup> · Heung Nam Han<sup>3</sup> · Sung-Tae Hong<sup>1</sup>

Received: 30 November 2023 / Revised: 1 March 2024 / Accepted: 5 March 2024 / Published online: 10 April 2024  
© The Author(s), under exclusive licence to Korean Society for Precision Engineering 2024

## Abstract

This study compares the electrically assisted pressure joining (EAPJ) performances of two non-ferrous alloys, aluminum (Al) 6061-T6 and copper (Cu) C11000. For joining, two cylindrical specimens with identical geometries are assembled in a longitudinal direction. Electric currents with various electric current densities are applied directly to the specimen assemblies during continuous axial plastic deformation. Microstructural analysis confirms that the joints are successfully fabricated without melting and solidification in both material combinations. While the mechanical properties of the joints are strongly affected by the electric current density, the results also show that both joining temperature and amount of plastic deformation for successful EAPJ of the C11000 alloy are much lower than those of the Al 6061-T6 alloy. In EAPJ, the Cu C11000 even can be joined at a temperature (250 °C) lower than the  $0.3\text{--}0.7T_m$  range ( $T_m$ : the melting temperature of material), while the Al 6061-T6 requires the joining temperature (450 °C), which is about  $0.7T_m$  for that material. The present study confirms that the process parameters for successful EAPJ can strongly differ depending on the metal alloy.

**Keywords** Electrically Assisted Pressure Joining · Current Density · Deformation · Temperature · Aluminum 6061-T6 · Copper C1100

## 1 Introduction

Depending on the industrial application, non-ferrous metal alloys offer advantages over ferrous alloys in terms of corrosion resistivity, thermal and electrical conductivity, and strength-to-weight ratios [1, 2]. The demand for complicated structural components made of non-ferrous metal alloys is increasing in various industrial applications. A proper joining technique for each non-ferrous alloy is essential to accomplish the target design.

Fusion joining has been commonly used to fabricate a joint of metallic materials. For example, arc welding can be applied in disparate workpiece positions and has been

preferable for welding of similar materials [3]. Laser welding also offers several advantages, including high energy density and welding speed, accurate control of heat input, and rapid cooling [4], all of which help reduce the size of heat-affected zone [5, 6]. However, fusion joining also has disadvantages, such as excessive thermal stress, residual stress, distortion, crack, and creation of a thick layer of intermetallic compounds (IMCs) after joining, resulting in severe deterioration of joint properties [7–9].

With the recent trend of using non-ferrous metal alloys, demand for solid-state joining, which can avoid the drawbacks of conventional fusion joining, is increasing. Among the popular processes for solid-state joining are pressure joining [10], friction joining [11, 12], and friction stir welding (FSW) [13–15]. Pressure joining has been considered an effective alternative to fusion joining due to its simplicity and cost-effectiveness. It has been demonstrated that workpieces for pressure joining need to undergo severe plastic deformation to break the oxide layer, which allows atom-to-atom contact and generates the bond. In cold pressure joining, the shape of the product may be severely altered due to the force required to induce plastic deformation. In conventional hot pressure joining, workpieces are heated in a furnace to reduce

✉ Sung-Tae Hong  
sthong@ulsan.ac.kr

<sup>1</sup> School of Mechanical Engineering, University of Ulsan, Ulsan, Republic of Korea

<sup>2</sup> Naval Architecture and Ocean Engineering College, Dalian Maritime University, Dalian, China

<sup>3</sup> Department of Materials Science and Engineering and Research Institute of Advanced Materials, Seoul National University, Seoul, Republic of Korea

the required joining force and to enhance diffusion. However, the heating process for conventional hot pressure joining is often time-consuming. Also, it is typically necessary to place the entire workpiece in the furnace, causing unexpected microstructural changes in the entire workpieces.

Friction joining offers benefits in overcoming the technical disadvantages of pressure joining since the heating and deformation during friction joining can be relatively localized compared with pressure joining. However, friction joining requires high-precision rotation and braking, which can be expensive and bulky. FSW, in which heat sources are purely mechanical, is a relatively well-commercialized process. However, it requires a complex and costly machine and a specially designed tool. Under these circumstances, a simple, efficient, and controllable joining method that provides acceptable joint properties with less damage to the vicinity of joint is needed.

Electrically assisted pressure joining (EAPJ) is a relatively new solid-state joining technique that avoids the drawbacks of conventional solid-state joining. With a certain amount of plastic deformation, EAPJ exploits thermal (resistance heating) and athermal [16] effects of electric current. EAPJ is highly efficient because the resistance heating and accompanying athermal effect of an electric current are rapid, localized, and controllable [17]. Also, since EAPJ does not require bulky (and expensive) rotation and braking systems, the entire system can be much more compact than conventional friction welding.

The athermal effect of electric current [16] reportedly enhances the atomic kinetics in microstructural rearrangements, such as recrystallization [18, 19], phase transformation [20, 21], and healing [22]. Kim et al. [16] reported that charge imbalances at microstructural defects weaken the strength of atomic bonding as an electric current is applied. Jeong et al. [23] reported that, as the current density increases for a fixed temperature, the athermal effect becomes more prominent. It is expected that the athermal effect can enhance the diffusion process during joining [24–29].

A sound solid-state joint was reportedly fabricated by means of EAPJ even for dissimilar material combinations with significantly different thermomechanical properties [25–27, 30]. Also, the effectiveness of EAPJ can be improved using an additive manufactured porous interlayer at the joining interface [28, 29]. Zhang et al. [29] reported that the additive layer has a measurable impact on the interfacial bond strength of EAPJed maraging steels/AISI stainless-steel joints. Lee et al. [31] successfully produced a robust joint of functionally graded lightweight steels (Mo-doped and Si-doped) by adopting EAPJ. They also reported that the chemical inhomogeneity matrix, which is typically observed in fusion joining, was avoided entirely. Furthermore, the concept of EAPJ can be simply expanded to in situ joining and forging, as demonstrated by Do et al. [32].

Although EAPJ has been actively investigated as mentioned above, few studies on the feasibility of EAPJ of various non-ferrous metal alloys have been conducted. Aluminum and copper are two typical face-centered-cubic structure metals that are commonly used in electrical industries. Unfortunately, the EAPJ performance of those two popular materials is still unclear. To fill this gap, EAPJ of aluminum (Al) 6061-T6 and copper (Cu) C11000 alloys and the efficiency of the joining process are compared in the present study. Especially, the joining performance and the microstructural evolution of joint are discussed in detail through microstructural analysis.

## 2 Experimental Set-Up

For the EAPJ experiment, cylindrical specimens of the Al 6061-T6 and C11000 alloys were used (each 10 mm in diameter and 10 mm in height), as shown in Fig. 1. The chemical compositions of both alloys are listed in Table 1. Silicon carbide (SiC) grinding paper (first a 180-grit paper followed by a 600-grit paper) was used to remove oxide layers on the joining surfaces. The specimens were degreased with acetone before the two cylindrical specimens were assembled along the axial direction. To minimize reoxidation of the joining surfaces, the interval between surface preparation and the EAPJ process was less than 1 min.

As shown in Fig. 2, a custom-made fixture for EAPJ was installed in a universal servo press machine with a capacity of 700 kN (DTU-800SP, Daekyoung, Busan, Republic of Korea). Both electrodes were made of tool steel. To isolate the servo press from the electric current, two insulators made of Bakelite were placed between the servo press and electrodes. A digital signal processor (DTU-2000X, Daekyoung, Busan, Republic of Korea) was used to record the load history and to control the displacement. A programmable electric current generator (VADAL SP-1000U, Hyosung, Seoul, Republic of Korea) connected to a cooling system supplied the current. An infrared thermal imaging camera (FLIR-T621, FLIR, Taby, Sweden) was used to record the temperature during the EAPJ process. Thermal black paint with heat resistance of up to 800 °C was sprayed on one

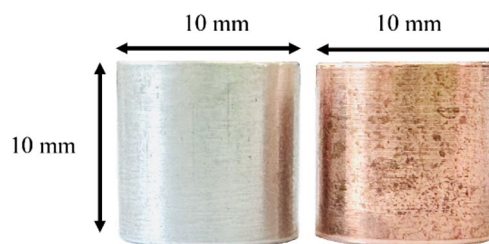
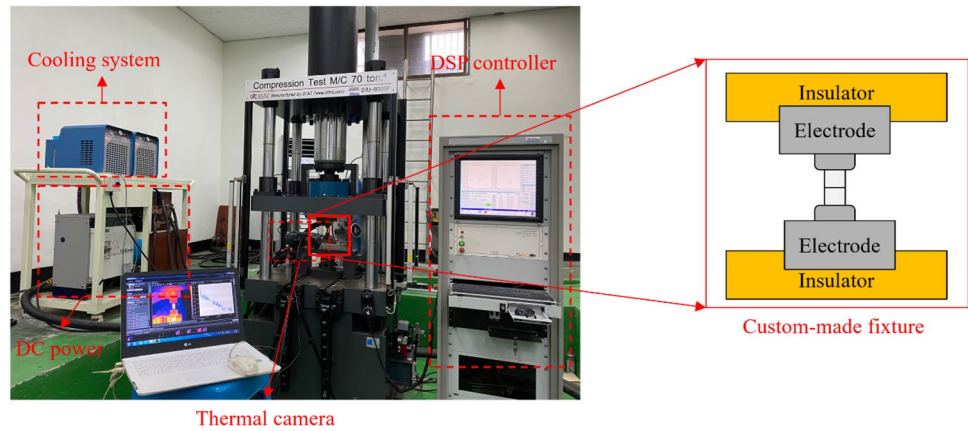


Fig. 1 The dimensions of specimens

**Table 1** Chemical composition of Al 6061 and C11000 alloys

Material	Chemical composition (wt%)								
	Si	Fe	Cu	Mn	Mg	Cr	Zn	Other	Al
AA6061-T6	0.67	0.5	0.23	0.12	0.9	0.17	0.07	0.02	Bal
C11000	-	-	99.95	-	-	-	-	Bal	-

**Fig. 2** The experimental set-up



**Table 2** The applied displacement, joining time, and target joining temperature in EAPJ

Displacement (mm)	Joining time (s)	Target joining temperature (°C)	
		Al/Al	Cu/Cu
5	23	330,450,550	250,350,550
10			
15			

side of the specimen surface to increase the accuracy of temperature measurements by stabilizing the emissivity. Before EAPJ, a 1000 N pre-load was applied to the specimen assembly to ensure firm contact between the specimens and between the specimen and electrode. As a result, sparks at the joining interface or at the interface between the specimen and electrode were effectively prevented when the electric current was applied.

To compare the EAPJ performance of Al/Al and Cu/Cu combinations, an applied displacement and target joining temperature were selected (Table 2). As schematically shown in Fig. 3, the displacement was set to complete concurrently with completion of the electric current. A displacement rate was chosen to maintain a constant joining time. In the present study, it was assumed that the effect of displacement rate on joining performance was not significant. A main current pulse was applied to reach the target joining temperature, and nine following pulses were applied to maintain the elevated temperature during the remaining joining time. The matrices of the electric current parameters for EAPJ of the Al/Al and Cu/Cu alloys, selected through

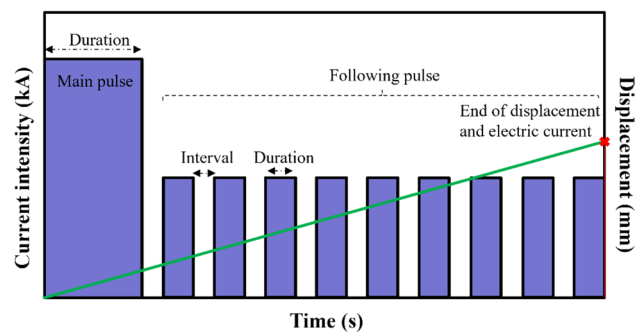


**Fig. 3** The schematic of electric current and displacement during EAPJ

preliminary tests, are listed in Table 3(a) and (b), respectively. Each set of parameters was tested at least three times to ensure repeatability.

After EAPJ, the joined samples were cut perpendicular to the interface (along the joining direction). The cross-sections were mechanically ground, polished, and then etched (Al/Al joint: H<sub>2</sub>O 190 mL, HNO<sub>3</sub> 5 mL, HCl 3 mL, HF 2 mL; Cu/Cu joint: H<sub>2</sub>O 50 mL, HNO<sub>3</sub> 50 mL) according to a typical metallographic preparation procedure. A field-emission scanning electron microscope (SU5000, Hitachi, Tokyo, Japan) equipped with an electron backscatter diffraction (EBSD) system (Velocity super/EDAX, California, USA) was used to observe the microstructure and to verify the absence of macroscopic defects in the joint. The EBSD analysis was carried out at the joint interface to investigate the microstructural evolution during joining. The working conditions for the EBSD analysis were 15 kV acceleration

**Table 3** Electric current parameters for EAPJ process

(a) Al/Al								
Max temperature* (°C)	Main pulse			Interval (s)	Following pulse			Total time (s)
	Intensity (kA)	Normal current density** (A/mm <sup>2</sup> )	Duration (s)		Intensity (kA)	Duration (s)	Number of pulse	
~330	3.2	40.74	5.0	0.5	3.2	1.5	9	23.0
~450	3.4	43.29			3.35			
~550	3.7	47.11			3.65			
(b) Cu/Cu								
Max temperature* (°C)	Main pulse			Interval (s)	Following pulse			Total time (s)
	Intensity (kA)	Normal current density** (A/mm <sup>2</sup> )	Duration (s)		Intensity (kA)	Duration (s)	Number of pulse	
~250	2.8	35.65	5.0	0.5	2.6	1.5	9	23.0
~350	3.2	40.74			3.2			
~550	5.0	63.66			4.0			

\* Approximate value reached at the end of main pulse

\*\* Defined as the current intensity of the main pulse divided by the original area of the workpiece

voltage, 18 mm working distance, a 70° tilt, and a 5° critical misorientation for grain identification. The microstructural evolution of EAPJ joints was analyzed through inverse pole figure (IPF), grain orientation spread (GOS), and kernel average misorientation (KAM) maps to obtain average grain sizes, recrystallization fractions, and KAM average values, respectively. Grains with a GOS between 0° and 2° were considered recrystallized grains. Finally, a Vickers indenter (HM-100, Mitutoyo, Kanagawa, Japan) was used to evaluate the mechanical properties. Vickers hardness (load: 1 N, dwell time: 10 s) was measured perpendicular to the joining interface with steps from the joint interface of 50 μm for the Al/Al joint and of 100 μm for the Cu/Cu joint.

### 3 Results and Discussion

#### 3.1 Process Response

The temperature and load histories of successful EAPJ of the selected materials are shown in Fig. 4. The temperature graphs of EAPJ displayed in Figs. 4a–c show a similar trend. When the main pulse of the electric current was applied, the temperature of the specimen assembly rapidly reached the target temperature. During the following nine current pulses, the temperature stayed at the elevated value, plateauing with serration. Finally, the specimen assembly was air-cooled. The induced temperature (the average temperature in the plateau) during the EAPJ process is referred to as the joining temperature. The load histories, as shown in Figs. 4d–f, during EAPJ of the two

materials exhibited similar trends overall. Initially, the load increased as a result of compressive displacement. As the temperature increased, the load began to decrease due to thermal softening of the joining materials. As the height of the specimen assembly continued to decrease due to compressive displacement (during the plateau of temperature), the load gradually increased. The load history clearly showed that the joining load decreased as the current density increased. Naturally, the load history during EAPJ of Al/Al showed lower values than those of Cu/Cu due to the different mechanical properties of the materials.

The joints were labeled according to the given experimental parameter sets (Fig. 5). For example, A-NT0.69D15 denotes a joint of AA6061/AA6061 at 69% of the normalized joining temperature, which was defined as the joining temperature divided by the melting temperature ( $T_m$ ) of the joining material, with 15 mm of compressive displacement.

For the combinations of displacement and joining temperature (or normalized joining temperature), the joining performances of the two material alloys were significantly different, as shown in the result maps (Fig. 6). The joining temperature and induced normalized temperature in the result maps are the average of three repeated tests. Among the displacement-temperature combinations selected in the present study, Al/Al joints were only produced with a displacement of 15 mm and normalized temperatures of 0.69 and 0.85. However, Cu/Cu joints were successfully created with displacements of 10 and 15 mm for all selected normalized temperatures. It is interesting to note that the EAPJ of copper was successful with a smaller

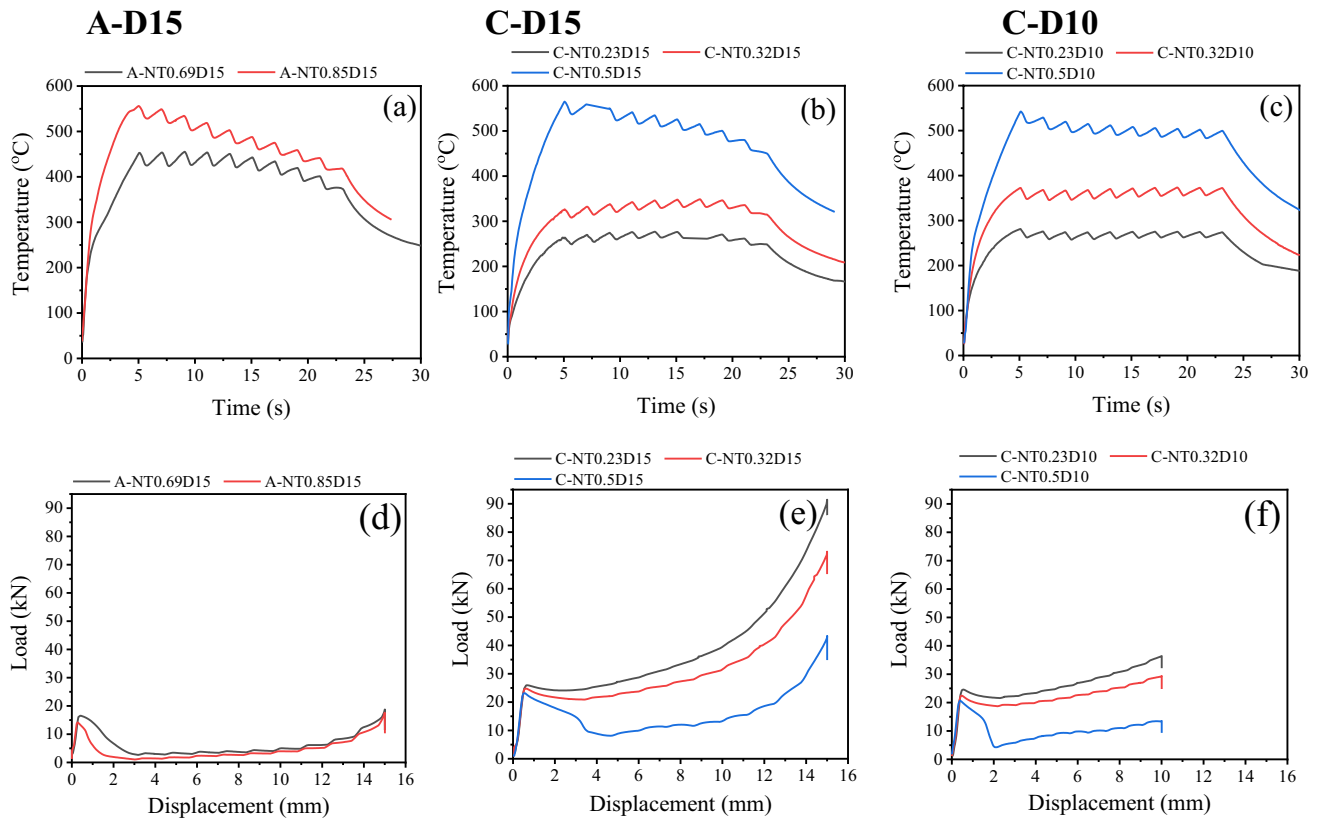


**Fig. 4** Histories of temperature (a,b,c) and load (d,e,f) during EAPJ of A-D15, C-D15, and C-D10, respectively

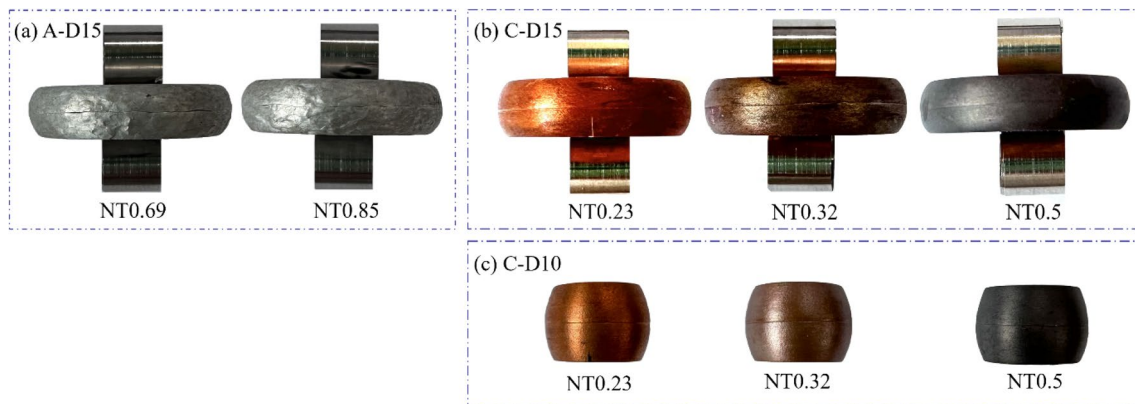


**Fig. 5** Successful joints: **a** Al/Al joints with 15 mm of displacement, **b** Cu/Cu joints with 15 mm of displacement, and **c** Cu/Cu joints with 10 mm of displacement

compressive displacement and at a lower temperature (for example, with a displacement of 10 mm at a joining temperature of 250 °C) compared with that of aluminum. A joining temperature of 250 °C, which induced successful EAPJ of copper, was even lower than the 0.3–0.7  $T_m$  range for diffusion-based solid-state joining during warm [33] and hot working [34].

### 3.2 AA6061/AA6061 Joint

IPF maps of as-received AA6061 and two cross-sections of joints are illustrated in Figs. 7a–c. The IPF maps of the A-NT0.69D15 and A-NT0.85D15 joints in Figs. 7b and c, respectively, show no detectable joint lines. A joint of similar materials is generally considered complete when the



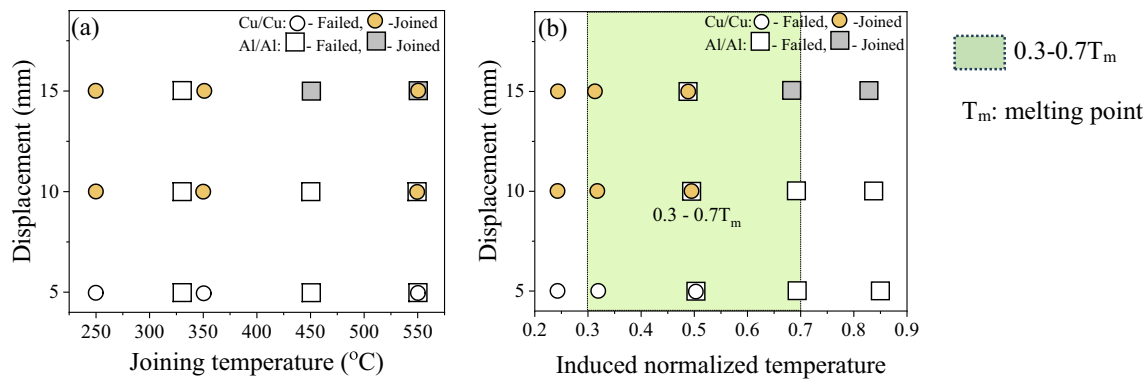


**Fig. 6** Result maps based on: **a** displacement vs temperature and **b** displacement vs induced normalized temperature

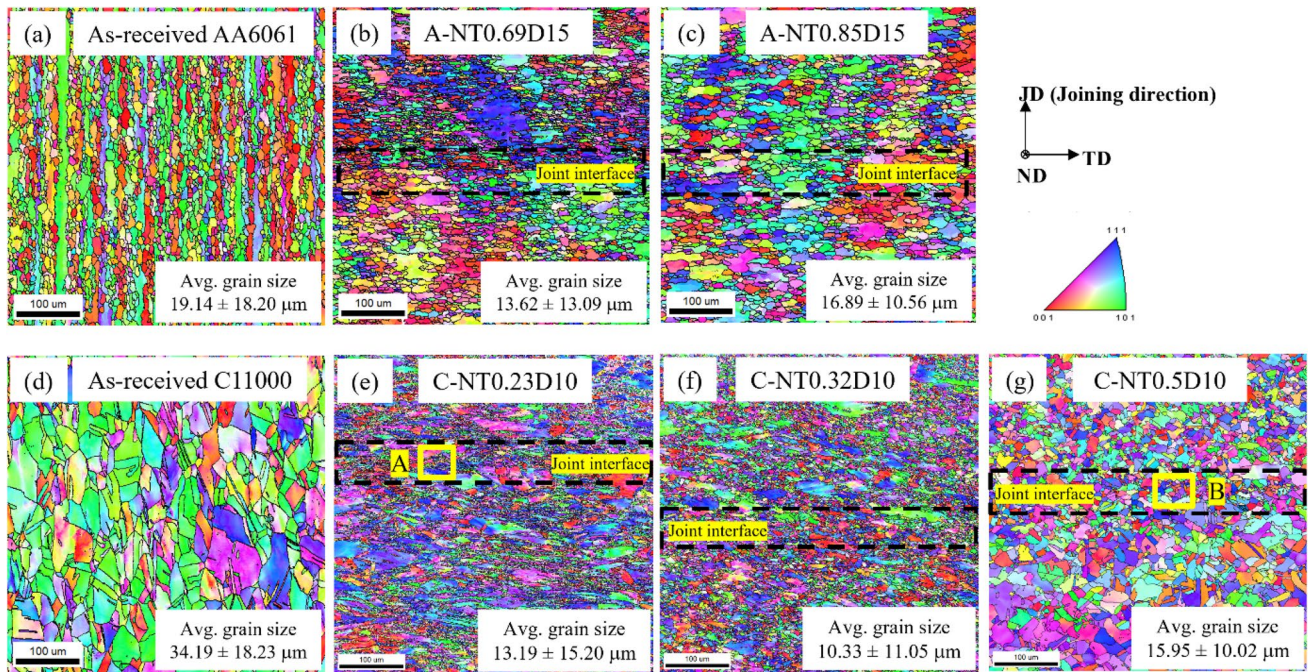


**Fig. 7** IPF maps of: **a** as-received AA6061, **b** A-NT0.69D15, **c** A-NT0.85D15, **d** as-received C11000, **e** C-NT0.23D10, **f** C-NT0.32D10, and **g** C-NT0.5D10

joining line is eliminated [35]. Additionally, EBSD observations show that neither joint had macroscopic defects nor a sign of melting or solidification in the joining interface. These results suggest that aluminum alloys were completely joined at a solid state in a relatively short time by EAPJ.

The average grain size of base materials and joints is listed in Table 4. The as-received AA6061 was composed of a mixture of elongated grains and equiaxed grains with an average grain size of  $19.14 \pm 18.20 \mu\text{m}$ , as detailed in Fig. 7a. The A-NT0.69D15 joint shown in Fig. 7b not only included compressed grains, but also consisted of many refined grains at the expense of deformed grains. This suggests that dynamic recrystallization (DRX) occurred during EAPJ, leading to

**Table 4** Average grain size of base materials and joints ( $\mu\text{m}$ )

As-received AA6061	A-NT0.69D15	A-NT0.85D15	-
$19.14 \pm 18.20$	$13.62 \pm 13.09$	$16.89 \pm 10.56$	-
As-received C11000	C-NT0.23D10	C-NT0.32D10	C-NT0.5D10
$34.09 \pm 18.23$	$13.19 \pm 15.20$	$10.33 \pm 11.05$	$15.95 \pm 10.02$

a decrease in average grain size ( $13.62 \pm 13.09 \mu\text{m}$ ). The microstructure of the A-NT0.85D15 joint in Fig. 7c shows that the joint consists of coarser grains (in comparison with the A-NT0.69D15 joint), with average grain size increasing to  $16.89 \pm 10.56 \mu\text{m}$ . Moreover, no distinct interfacial lines

were observed at the joining interface (the so-called interfacial grain boundary [IGB]) [36, 37], which differs from the A-NT0.69D15 joint interface. The loss of IGBs can be explained by the formation of triple junctions between grains across the interface and by rapid grain growth, resulting in a complete joint [36]. This suggests that an increase in normalized temperature, corresponding with an increase in current density, accelerated the diffusion of atoms across the interface and enhanced the migration of IGBs.

Figures 8a-c depict GOS maps of the base material and EAPJed AA6061. Recrystallized grains are indicated in green ( $0 < \text{GOS} < 1^\circ$ ) and blue ( $1 < \text{GOS} < 2^\circ$ ). The DRX fraction of the A-NT0.69D15 and A-NT0.85D15 joints

was similar, at 43.88% and 40.58%, respectively. However, the hardness value of the two joints was significantly lower than that of the base material (117 HV), as shown in Fig. 9a. This can be attributed to elevated temperatures induced by the electric current, which dissolved the strengthening precipitates in the Al–Mg–Si alloy, leading to a degradation in hardness after EAPJ [26]. As shown in Fig. 9a, the hardness of the A-NT0.69D15 joint was greater than that of the A-NT0.85D15 joint at all measured steps, despite similar DRX fractions. This is because the A-NT0.69D15 joint was subjected to a lower temperature, resulting in lower grain growth in the former joint (Fig. 7).

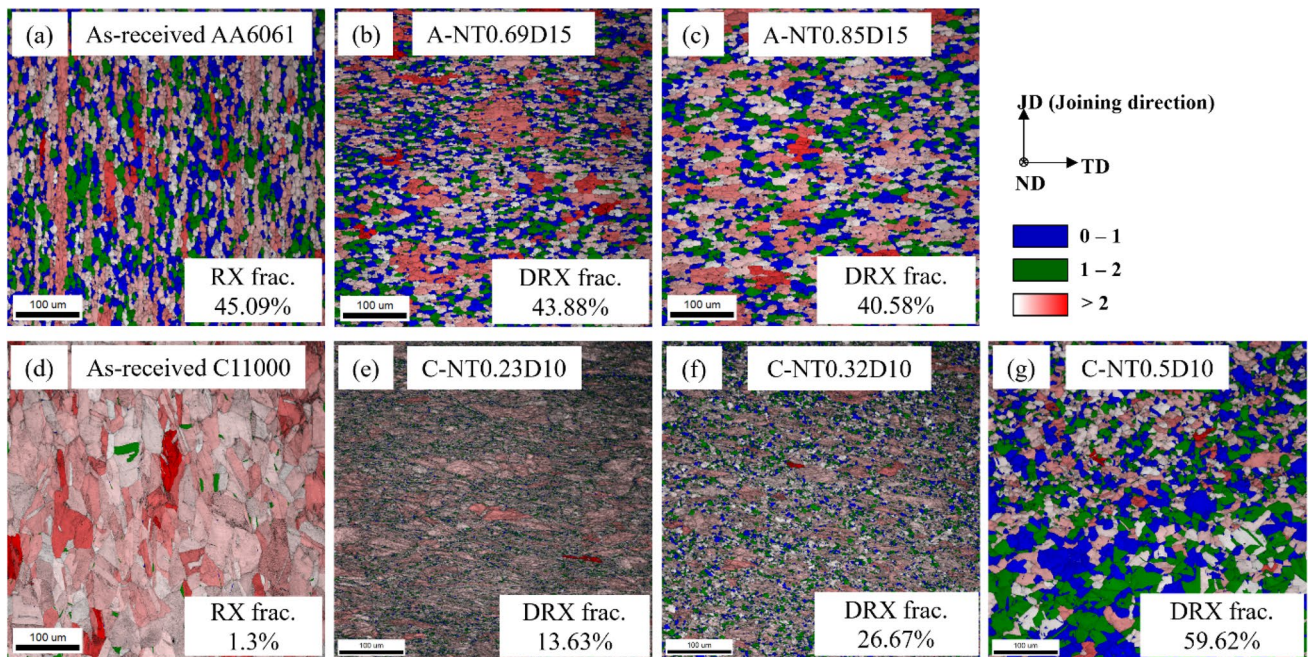
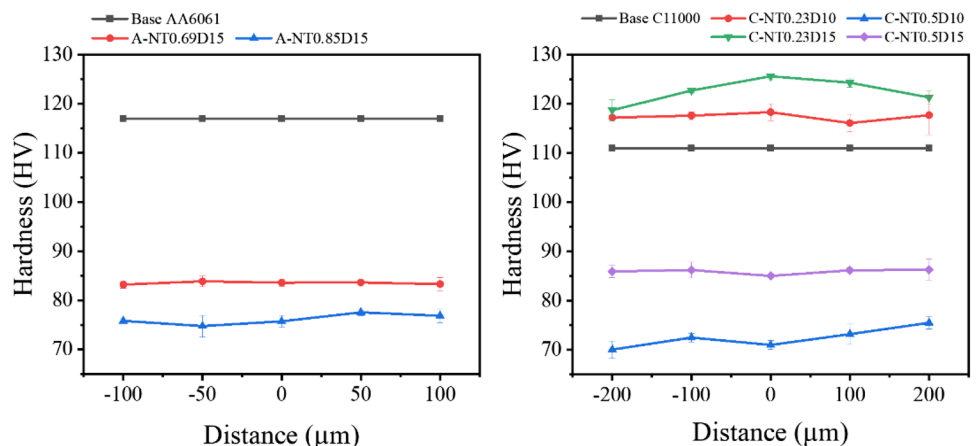


**Fig. 8** GOS maps of **a** as-received AA6061, **b** A-NT0.69D15, **c** A-NT0.85D15, **d** as-received C11000, **e** C-NT0.23D10, **f** C-NT0.32D10, and **g** C-NT0.5D10

**Fig. 9** Hardness response of as-received materials and joining interface: **a** Al/Al joint and **b** Cu/Cu joint





### 3.3 C11000/C11000 Joint

In terms of efficiency, C-D10 joints were used to carry out the comparative microstructural analysis with respect to the Al/Al joints, as C-D10 joints can be produced at a much lower total energy than C-D15 joints. Figures 7d–g show the IPF maps of as-received C11000 and C-D10 joints. The successful creation of C-D10 joints was confirmed through IPF maps, as depicted in Figs. 7e–g, which clearly show that the joint line of these joints is unidentified. This confirms that EAPJ can be adapted to create a complete solid joint of copper C11000 alloys with less plastic deformation and at a lower temperature, which also corresponds to lower normalized temperature, compared with the AA6061 alloy.

An IPF map of the as-received copper, shown in Fig. 7d, reveals the microstructure of equiaxed grains, including some twins, with an average grain size of  $34.19 \pm 18.23 \mu\text{m}$ . The IPF map of the C-NT0.23D10 joint clearly shows a large number of refined grains near the joint interface, while the matrix of both sides includes a combination of large amounts of compressed fibrous grains and refined grains, as shown in Fig. 7e. The average grain size of the joint was reduced significantly to  $13.19 \pm 15.20 \mu\text{m}$ . Specifically, the grain boundaries of the deformed grains in the matrix appeared to be bulging where the nuclei prefer to be formed [33]. Figure 7f shows that the C-NT0.32D10 joint is composed of refined grains (larger than the C-NT0.23D10 joint) and a higher volume fraction of DRX-ed grains compared with the C-NT0.23D10 joint, resulting in a reduction of fibrous grains. The average grain size was reduced slightly to  $10.33 \pm 11.05 \mu\text{m}$ . In addition, the joint interface of the C-NT0.32D10 joint was accompanied primarily by the formation and growth of refined DRX-ed grains. Figure 7g shows that the C-0.5NTD10 joint is composed of uniform equiaxed and coarse grains, leading to an increase in average grain size ( $15.95 \pm 10.02 \mu\text{m}$ ). Specifically, some grains apparently grew across the interface (marked by a yellow square box), which is evidence of the migration of IGB [35].

It is clear that the extent of DRX was enhanced as current density increased during EAPJ.

To confirm the elimination mechanism of the joint line, the IPF maps of the C-NT0.23D10 and C-NT0.5D10 joints were enlarged to observe the evolution at the joint interface. Figure 10 shows the enlarged IPF maps of yellow square boxes A and B in Figs. 7e and g, respectively. The IPF map of the C-NT0.23D10 joint in Fig. 10a shows clear evidence of new refined grains at the bulging grain boundaries (black dash-dot area). The joint line is also composed of many refined grains and some coarse grains, which extend to two sides of the interface. Figure 10b clearly demonstrates no joint line of the C-NT0.5D10 due to the existence of coarse grains across the joining interface. This suggests that the electric current density strongly assisted the grain growth. The EBSD observation confirms the initiation of recrystallization and grain growth at the interface under the assistance of electric current, which contributed to the migration of IGBs and led to the elimination of the joint line and creation of a complete joint.

Analogous to the GOS value of the aluminum section, the grains can be defined as recrystallized as the GOS value is lower than  $2^\circ$  (green:  $0 < \text{GOS} < 1^\circ$ , and blue:  $1 < \text{GOS} < 2^\circ$ ), as depicted in Fig. 8. The recrystallization fraction of the as-received material was 1.3%, as shown in Fig. 8d. After EAPJ at NT0.23D10, the fraction of DRX-ed grains of the joint increased significantly (13.63%). As the current density increased, the size and fraction of DRX grains (26.67% and 59.62%) increased dramatically throughout the C-NT0.32D10 and C-0.5NTD10 joints, as shown in Figs. 8f–g, respectively. Specifically, the DRX-ed grains surrounded deformed grains in the C-NT0.23D10 and C-NT0.32D10 joints, while the C-NT0.5D10 showed a near complete loss of deformed grains. The hardness at the joining area of the C-D10 and C-D15 joints was measured and plotted in Fig. 9b. For the C-D10 case, the hardness value of the C-NT0.23D10 joint was greater than that of the as-received material even though the fraction

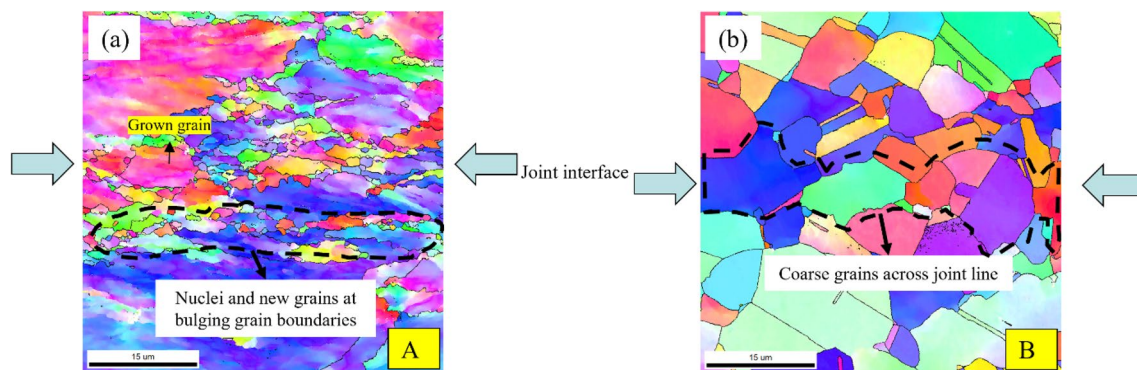
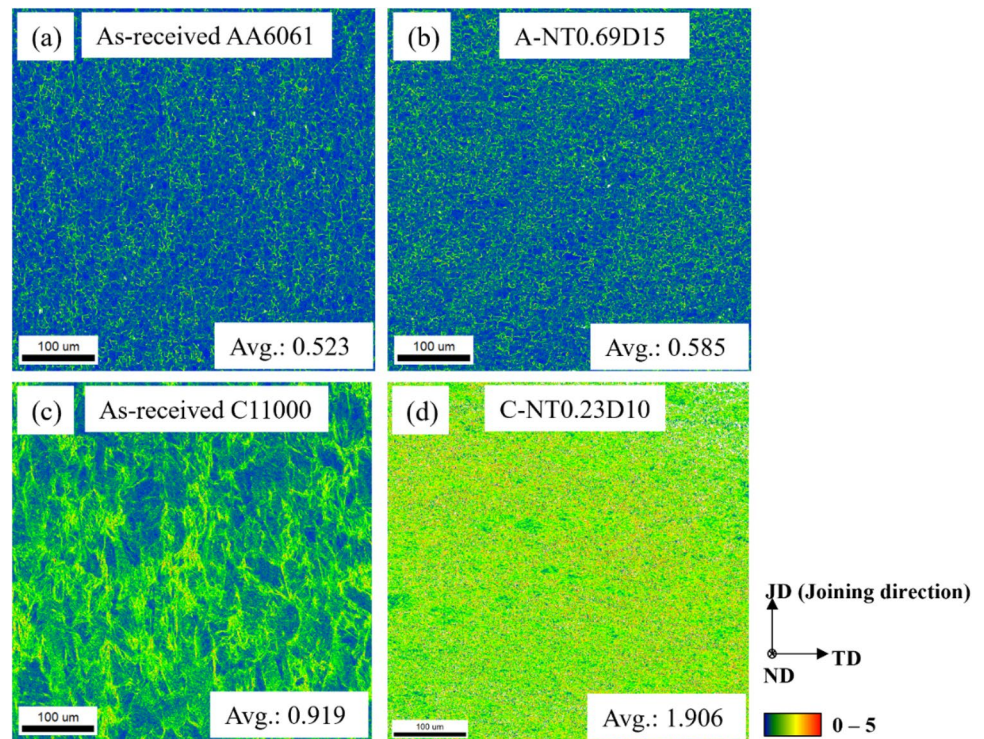


**Fig. 10** The enlarged IPF maps of the yellow boxes A and B in Fig. 7: **a** C-NT0.23D10 and **b** C-NT0.5D10



**Fig. 11** KAM maps of: **a** as-received AA6061, **b** A-NT0.69D15, **c** as-received C11000, and **d** C-NT0.23D10



of recrystallization was higher due to strain hardening of the NT0.23D10 joint. In contrast, the hardness value of the C-NT0.5D10 joint intensely decreased due to dynamic recrystallization and the disappearance of deformed grains at higher joining temperatures. The hardness of the C-D15 joints at the joining interface was also measured. The hardness of the C-D15 joints was higher than that of C-D10 joints when the normalized temperature was the same. This can be explained by greater plastic deformation of the C-D15 joints compared with the C-D10 joints, causing higher strain hardening [38].

The difference in the amount of applied displacement and the joining temperature for successful EAPJ of Al/Al and Cu/Cu can be explained by the hypothesis based on the difference in stacking fault energy (SFE): aluminum is a high-SFE material, while copper is a medium-SFE material. The dislocation density of the high-SFE material (aluminum) produced during plastic deformation is significantly lower than that of the low- to medium-SFE material (copper) [39]. The dislocation is a source of the diffusion path as well as the grain boundary migration [40]. Also, a higher dislocation density can enhance the charge-imbalance effect of electric current [16]. Since the geometrically necessary dislocation can be represented by the local misorientation (KAM value), KAM maps can be used to indicate the existence of dislocation density [41, 42]. KAM maps of as-received materials and the joining area of A-NT0.69D15 and C-NT0.23D10 joints are displayed in Fig. 11. The KAM value of aluminum increased slightly from 0.523 to 0.585 (11.85%), while that

of copper increased from 0.919 to 1.906 (107.40%) after EAPJ, even though the amount of compressive displacement in C-NT0.23D10 was 50% lower than that of A-NT0.69D15. The KAM maps confirm that the induced dislocation density during EAPJ of copper was much higher than that of aluminum. Therefore, the Al/Al workpiece should undergo greater deformation compared with Cu/Cu to produce a similar amount of dislocation, which facilitates joining. This explains why the EAPJ of Cu/Cu can be successfully conducted with a lower compressive displacement and/or a lower joining temperature compared to that of Al/Al.

## 4 Conclusion

Two non-ferrous alloys, aluminum 6061-T6, and copper C11000, were successfully joined in a short time using EAPJ without melting and solidification. A comparison of EAPJ performances of the selected materials was conducted through microstructural analysis. The results show that both joining temperature and amount of plastic deformation for successful EAPJ of copper C11000 were much lower than those of aluminum 6061-T6. The temperature for successful EAPJ of C1000 was even lower than the range for diffusion-based solid-state joining ( $0.3\text{--}0.7T_m$ ). These results might be explained by the hypothesis based on the difference in SFE. The results of the present study confirm that the process parameters for successful EAPJ can differ strongly depending on the metal alloy. EBSD observation clearly confirms

that the complete joint was created as the increased normalized temperature (as a result of increased current density) enhanced the recrystallization and grain growth process, followed by the migration of IGBs. The mechanical properties of the joint are measured by the hardness value, which is strongly affected by the process parameters. This study confirms that EAPJ is promising and applicable to joining of non-ferrous metals.

**Acknowledgements** This work was supported by National Research Foundation of Korea (NRF) grant funded by the Korea government (MSIT) (No. 2019R1A2C2009939, 2021R1A2C3005096). This work was also supported by "Regional Innovation Strategy (RIS)" through the National Research Foundation of Korea (NRF) funded by the Ministry of Education (MOE)(2021RIS-003).

**Data Availability** The raw/processed data required to reproduce these findings cannot be shared at this time as the data are part of an ongoing study.

## Declarations

**Competing Interest** The authors report no conflict of interest.

## References

- Liu, L., Ren, D., & Liu, F. (2014). A review of dissimilar welding techniques for magnesium alloys to aluminum alloys. *Materials*, 7(5), 3735–3757. <https://doi.org/10.3390/ma7053735>
- Sahin, M. (2010). Joining of aluminium and copper materials with friction welding. *International Journal of Advanced Manufacturing Technology*, 49(5–8), 527–534. <https://doi.org/10.1007/s00170-009-2443-7>
- Sahoo, A., & Tripathy, S. (2019). Development in plasma arc welding process: A review. *Materials Today: Proceedings*, 41, 363–368. <https://doi.org/10.1016/j.matpr.2020.09.562>
- Liu, F., Chen, T., Pang, L., Song, K., & Wu, Y. (2022). Study on Electro-Spark Deposition Welding of Ultra-thin Sheet of Ti-6.5Al-1Mo-1 V-2Zr Alloy. *International Journal of Precision Engineering and Manufacturing*, 23(10), 1203–1210. <https://doi.org/10.1007/s12541-022-00699-y>
- Wang, P., Chen, X., Pan, Q., Madigan, B., & Long, J. (2016). Laser welding dissimilar materials of aluminum to steel: An overview. *International Journal of Advanced Manufacturing Technology*, 87(9–12), 3081–3090. <https://doi.org/10.1007/s00170-016-8725-y>
- Kwak, Y., Kang, T., Lee, S. H., & Kang, M. (2023). Effects of Laser and Tungsten Arc Welding Processes on the Thermal Softening and Mechanical Properties of Almag6 Aluminum Alloy. *International Journal of Precision Engineering and Manufacturing*, 24(4), 531–536. <https://doi.org/10.1007/s12541-023-00772-0>
- Ueda, Y., Murakawa, H., & Ma, N. (2012). Introduction to Welding Mechanics. In *Welding Deformation and Residual Stress Prevention*. <https://doi.org/10.1016/b978-0-12-394804-5.00001-3>
- Atabaki, M. M., Nikodinovski, M., Chenier, P., Ma, J., Harooni, M., & Kovacevic, R. (2014). Welding of Aluminum Alloys to Steels: An Overview. *Journal for Manufacturing Science and Production*, 14(2), 59–78. <https://doi.org/10.1515/jmsp-2014-0007>
- Zhao, S., & Li, Y. (2023). Numerical Analysis of Welding Direction and Sequence for Controlling Distortion and Residual Stress in Aluminum Plate-Sleeve Structures. *International Journal of Precision Engineering and Manufacturing*, 24(6), 1011–1031. <https://doi.org/10.1007/s12541-023-00794-8>
- Mohamed, H. A., & Washburn, J. (1975). Mechanism of Solid State Pressure Welding. *Welding Journal (Miami, Fla)*, 54(9), 302–310.
- Kang, J. W., Zhang, S., Bui Thi, T. A., Hong, S. T., Lee, S., & Han, H. N. (2023). Friction-Assisted Dissimilar Solid State Lap Joining of Aluminum and Copper Pipes. *International Journal of Precision Engineering and Manufacturing*, 24(2), 199–208. <https://doi.org/10.1007/s12541-022-00745-9>
- Kim, G. W., Song, K. H., & Jeong, S. M. (2022). Realization of Enhanced Mechanical Properties of Solid-State Welded Ti Alloy with Commercial Purity. *International Journal of Precision Engineering and Manufacturing*, 23(5), 471–477. <https://doi.org/10.1007/s12541-022-00633-2>
- Laska, A., Szkodo, M., Pawłowski, Ł., & Gajowiec, G. (2023). Corrosion Properties of Dissimilar AA6082/AA6060 Friction Stir Welded Butt Joints in Different NaCl Concentrations. *International Journal of Precision Engineering and Manufacturing - Green Technology*, 10(2), 457–477. <https://doi.org/10.1007/s40684-022-0441-z>
- Basak, S., Mondal, M., Gao, K., Hong, S. T., Anaman, S. Y., & Cho, H. H. (2022). Friction stir butt-welding of roll clad aluminum thin sheets: effect of microstructural and texture changes on mechanical properties. *Materials Science and Engineering: A*, 832, 142490. <https://doi.org/10.1016/j.msea.2021.142490>
- Hammood, A. S., Esmailzadeh, M., Hosseini, S. N., Karimi, S., Calliari, I., Pezzato, L., & Brittain, R. (2023). Effect of Friction Stir Welding Parameters on Microstructure and Corrosion Behavior of 2101 Duplex Stainless Steel in Simulated Body Fluid. *International Journal of Precision Engineering and Manufacturing - Green Technology*, 10(2), 327–337. <https://doi.org/10.1007/s40684-022-00440-0>
- Kim, M. J., Yoon, S., Park, S., Jeong, H. J., Park, J. W., Kim, K., Jo, J., Heo, T., Hong, S. T., Cho, S. H., Kwon, Y. K., Choi, I. S., Kim, M., & Han, H. N. (2020). Elucidating the origin of electroplasticity in metallic materials. *Applied Materials Today*, 21, 100874. <https://doi.org/10.1016/j.apmt.2020.100874>
- Lupi, S., Forzan, M., & Alifirov, A. (2015). Analytical and Numerical Methods for Calculation of Induction and Conduction Heating Systems. In *Induction and Direct Resistance Heating*. [https://doi.org/10.1007/978-3-319-03479-9\\_5](https://doi.org/10.1007/978-3-319-03479-9_5)
- Park, J. W., Jeong, H. J., Jin, S. W., Kim, M. J., Lee, K., Kim, J. J., Hong, S. T., & Han, H. N. (2017). Effect of electric current on recrystallization kinetics in interstitial free steel and AZ31 magnesium alloy. *Materials Characterization*, 133(September), 70–76. <https://doi.org/10.1016/j.matchar.2017.09.021>
- Nguyen, T. A. N., Choi, H., Kim, M. J., Hong, S. T., & Han, H. N. (2022). Evaluation of Efficiency of Electrically Assisted Rapid Annealing Compared to Rapid Induction Heat Treatment. *International Journal of Precision Engineering and Manufacturing - Green Technology*, 9(2), 485–492. <https://doi.org/10.1007/s40684-021-00382-z>
- Ben, D. D., Yang, H. J., Ma, Y. R., Shao, X. H., Pang, J. C., & Zhang, Z. F. (2018). Rapid hardening of AISI 4340 steel induced by electropulsing treatment. *Materials Science and Engineering A*, 725(January), 28–32. <https://doi.org/10.1016/j.msea.2018.04.013>
- Zeng, B., Yan, X., Xie, Z., Liu, J., Wang, J., Huang, K., & Yang, Y. (2023). Plastic Deformation Mechanism of the Ti6Al4V Microgear Formed Under an Electrical Field. *International Journal of Precision Engineering and Manufacturing - Green Technology*, 11(1), 107–122. <https://doi.org/10.1007/s40684-023-00536-1>
- Jeong, H. J., Kim, M. J., Choi, S. J., Park, J. W., Choi, H., Luu, V. T., Hong, S. T., & Han, H. N. (2020). Microstructure reset-based self-healing method using sub-second electric pulsing for metallic materials. *Applied Materials Today*, 20, 100755. <https://doi.org/10.1016/j.apmt.2020.100755>

23. Jeong, K., Jin, S.-W., Kang, S.-G., Park, J.-W., Jeong, H.-J., Hong, S.-T., Cho, S. H., Kim, M.-J., & Han, H. N. (2022). Athermally Enhanced Recrystallization Kinetics of Ultra-Low Carbon Steel via Electric Current Treatment. *Acta Materialia*, 232, 117925. <https://doi.org/10.1016/j.actamat.2022.117925>
24. Zhang, S., Cai, L., Nguyen, T. A. N., Geng, M., Gao, K., Hong, S. T., & Kim, M. J. (2023). Effects of Intermetallic Evolution by Electrically Assisted Rapid Heat Treatment on the Mechanical Performance and Formability of Aluminum Clad Steel. *International Journal of Precision Engineering and Manufacturing - Green Technology*, 10(2), 367–379. <https://doi.org/10.1007/s40684-022-00460-w>
25. Li, Y. F., Das, H., Hong, S. T., Park, J. W., & Han, H. N. (2018). Electrically assisted pressure joining of titanium alloys. *Journal of Manufacturing Processes*, 35(June), 681–686. <https://doi.org/10.1016/j.jmapro.2018.09.015>
26. Zhang, S., Gao, K., Hong, S. T., Ahn, H., Choi, Y., Lee, S., & Han, H. N. (2021). Electrically assisted solid state lap joining of dissimilar steel S45C and aluminum 6061–T6 alloy. *Journal of Materials Research and Technology*, 12, 271–282. <https://doi.org/10.1016/j.jmrt.2021.02.091>
27. Akmal, M., et al. (2024). Achieving Superior Strength and Elongation from Electrically Assisted Pressure Joining of Medium Entropy Alloy and Ti-6Al-4V. *Scripta Materialia*, 239(September 2023), 115781. <https://doi.org/10.1016/j.scriptamat.2023.115781>
28. Hong, S. T., Li, Y. F., Park, J. W., & Han, H. N. (2018). Effectiveness of electrically assisted solid-state pressure joining using an additive manufactured porous interlayer. *CIRP Annals*, 67(1), 297–300. <https://doi.org/10.1016/j.cirp.2018.04.062>
29. Zhang, S., Van Loi, T., Boakye, S. Y., Anaman, S. Y., Cai, L., Gao, K., Hong, S. T., Cho, H. H., & Kim, D. H. (2022). Effectiveness of an additively manufactured porous layer in dissimilar solid-state bulk joining of additively manufactured maraging steel and conventional AISI410 steel. *Additive Manufacturing*, 49(November), 102508. <https://doi.org/10.1016/j.addma.2021.102508>
30. Anh, T., Nguyen, N., Basak, S., Zhang, S., Thuong, T., & Mounarik, D. (2022). Electrically assisted pressure joining of thin bi-layer aluminum - clad aluminum sheets. *The International Journal of Advanced Manufacturing Technology*, 4713–4723. <https://doi.org/10.1007/s00170-022-09687-y>
31. Lee, S., et al. (2024). Development of Functionally Graded Austenitic Lightweight Steel through Electrically Assisted Pressure Solid-State Joining. *Materials Science and Engineering: A*, 891(September 2023), 146003. <https://doi.org/10.1016/j.msea.2023.146003>
32. Do, T. T., Lee, S., Tu, T., Bui, A., Anh, T., Nguyen, N., Lee, J., Han, H. N., & Hong, S. (2022). *Simultaneous Joining and Forming of Dissimilar Steels by Electrically Assisted Pressure Joining.*, 2200256, 1–8. <https://doi.org/10.1002/srin.202200256>
33. Khan, H. A., Asim, K., Akram, F., Hameed, A., Khan, A., & Mansoor, B. (2021). Roll bonding processes: State-of-the-art and future perspectives. *Metals*, 11(9), 1344. <https://doi.org/10.3390/met11091344>
34. Vural, M. (2014). *Welding Processes and Technologies*. In *Comprehensive Materials Processing* (Vol. 6). Elsevier. <https://doi.org/10.1016/B978-0-08-096532-1.00603-8>
35. Zhang, J. Y., Sun, M. Y., Xu, B., Hu, X., Liu, S., Xie, B. J., & Li, D. Z. (2019). Evolution of the interfacial microstructure during the plastic deformation bonding of copper. *Materials Science and Engineering A*, 746(November 2018), 1–10. <https://doi.org/10.1016/j.msea.2018.12.119>
36. Huang, Y., Ridley, N., Humphreys, F. J., & Cui, J. Z. (1999). Diffusion bonding of superplastic 7075 aluminium alloy. *Materials Science and Engineering A*, 266(1–2), 295–302. [https://doi.org/10.1016/s0921-5093\(98\)00958-7](https://doi.org/10.1016/s0921-5093(98)00958-7)
37. Alhazaa, A., Haneklaus, N., & Almutairi, Z. (2021). Impulse pressure-assisted diffusion bonding (IPADB): *Review and outlook*. *Metals*, 11(2), 1–9. <https://doi.org/10.3390/met11020323>
38. Shabani, A., Bagheri, A., Toroghinejad, M. R., & Cavaliere, P. (2024). Texture Evolution and Hardening Behavior of Al/IF Composite Produced through Severe Plastic Deformation. *Materials Science and Engineering: A*, 889(November 2023), 145816. <https://doi.org/10.1016/j.msea.2023.145816>
39. Deshpande, A., Tofangchi, A., & Hsu, K. (2019). Microstructure evolution of Al6061 and copper during ultrasonic energy assisted compression. *Materials Characterization*, 153(April), 240–250. <https://doi.org/10.1016/j.matchar.2019.05.005>
40. Pelleg, J. (2016). Diffusion in dislocations. *Solid Mechanics and Its Applications*, 221, 87–94. [https://doi.org/10.1007/978-3-319-18437-1\\_8](https://doi.org/10.1007/978-3-319-18437-1_8)
41. Ha, C., Bohlen, J., Yi, S., Zhou, X., Brokmeier, H. G., Schell, N., Letzig, D., & Kainer, K. U. (2019). Influence of Nd or Ca addition on the dislocation activity and texture changes of Mg–Zn alloy sheets under uniaxial tensile loading. *Materials Science and Engineering A*, 761(June), 138053. <https://doi.org/10.1016/j.msea.2019.138053>
42. Rui, S. S., Han, Q. N., Wang, X., Li, S., Ma, X., Su, Y., Cai, Z., Du, D., & Shi, H. J. (2021). Correlations between two EBSD-based metrics Kernel Average Misorientation and Image Quality on indicating dislocations of near-failure low alloy steels induced by tensile and cyclic deformations. *Materials Today Communications*, 27(April), 102445. <https://doi.org/10.1016/j.mtcomm.2021.102445>

**Publisher's Note** Springer Nature remains neutral with regard to jurisdictional claims in published maps and institutional affiliations.

Springer Nature or its licensor (e.g. a society or other partner) holds exclusive rights to this article under a publishing agreement with the author(s) or other rightsholder(s); author self-archiving of the accepted manuscript version of this article is solely governed by the terms of such publishing agreement and applicable law.



**Tu-Anh Bui-Thi** Ph.D. candidate in the School of Mechanical Engineering, University of Ulsan. Her research interests are electrically assisted manufacturing and electrically assisted pressure joining of similar and dissimilar materials.



**Thanh Thuong Do** Ph.D. candidate in the School of Mechanical Engineering, University of Ulsan. His research interests are electrically assisted pressure joining and forming of metallic materials.





**Shengwei Zhang** A lecturer at Naval Architecture and Ocean Engineering College, Dalian Maritime University, China. He received his Ph.D. in mechanical and automobile engineering from University of Ulsan, South Korea. His research interests include metal forming, electrically assisted manufacturing, and solid state joining.



**Heung Nam Han** Professor in Department of Materials Science and Engineering, Seoul National University. His research interest is the mechanical behaviour and microstructure characterization for materials.



**Yijae Kim** Ph. D candidate in Department of Materials Science and Engineering, Seoul National University. Her research interests lie in analyzing the effects of electric currents on metallic materials from both mechanical and microstructural perspectives.



**Sung-Tae Hong** Professor in the School of Mechanical Engineering at the University of Ulsan, South Korea. His research interests include metal forming, electrically assisted manufacturing, and solid state joining.